Journal of King Saud University – Engineering Sciences (2016) xxx, xxx–xxx

King Saud University

Journal of King Saud University – Engineering Sciences

www.ksu.edu.sa
www.sciencedirect.com

ORIGINAL ARTICLES

Ultra-clean hydrogen production by ammonia decomposition

M.E.E. Abashar *

Chemical Engineering Department, College of Engineering, King Saud University, P.O. Box 800, Riyadh 11421, Saudi Arabia

Received 30 August 2015; accepted 13 January 2016

KEYWORDS

Ammonia decomposition;
Hydrogen;
Inter-stage heating;
Membrane reactor;
Modeling;
Multi-stage reactors

Abstract A rigorous heterogeneous mathematical model is used to simulate a cascade of multi-stage fixed bed membrane reactors (MSFBMR) with inter-stage heating and fresh sweep gas for the decomposition of ammonia to produce high purity hydrogen suitable for the PEM fuel cells. Different reactor configurations are compared. The comparison between a single fixed bed reactor (FBR) and a single fixed bed membrane reactor (FBMR) shows that the FBMR is superior to the FBR and gives 60.48% ammonia conversion higher than the FBR. However, 20.91% exit ammonia conversion obtained by the FBMR is considered to be poor. The FBMR is limited by the kinetics at low temperatures. The numerical results show that the MSFBMR of four beds achieve 100.0% ammonia conversion. It was found that the membrane plays the prime role in the displacement of the thermodynamic equilibrium. The results also show that, a linear relationship exists between the number of beds and the feed temperature and a correlation has been developed. A critical point for an effective hydrogen permeation zone has been identified. It is observed that the diffusion limitation is confined to a slim region at the entrance of the reactor. It is also observed that the heat load assumes a maximum inflection point and explanations offered. The results show that the multi-stage configuration has a promising potential to be applied successfully on-site for ultra-clean hydrogen production.

1. Introduction

Ultra-clean hydrogen has been recognized as a carbon-free fuel that can be used to power polymer electrolyte membrane (PEM) fuel cells. The PEM fuel cell is an efficient electrochemical device that produces electricity that can be used in several important applications such as transportation, power generation and electronic devices (Zamel, 2013). Although the PEM fuel cells are a versatile clean technology and friendly to the environment, but are sensitive to hydrogen purity. Carbon monoxide traces of about (5–10 ppm) are enough to severely poison the active sites of the platinum catalyst at the anode, resulting in transient cell potential oscillations and a profound drop in the overall efficiency of the PEM fuel cell (Oetjen et al., 1996; Farrell et al., 2007). Also, ammonia traces of about 13 ppm have catalyst poisoning effects on the PEM

* Fax: +966 1 4678770.
E-mail address: mabashar@ksu.edu.sa

Peer review under responsibility of King Saud University.

ELSEVIER Production and hosting by Elsevier

http://dx.doi.org/10.1016/j.jksues.2016.01.002

Nomenclature

A_o	reactor area, m^2
C	total concentration, kmol/m^3
C_i	concentration of component i, kmol/m^3
C_{pi}	specific heat of component i, kJ/kmol K
C_{pmix}	gas specific heat, kJ/kg °C
d_{H2}	diameter of hydrogen membrane tube (m)
D_i	bulk diffusion coefficient of component i, m^2/h
D_i^o	diffusion coefficient of component i at 0 °C and 1 atm, m^2/h
D_{ji}^o	diffusion coefficient of component j in component i, m^2/h
D_{ei}	effective diffusion coefficient of component i, m^2/h
f_i	fugacity of component i
F_i	molar flow rate of component i, kmol/h
F_i^o	initial molar flow rate of component i, kmol/h
ΔH	enthalpy change of reaction, kJ/kmol
K	equilibrium constant, kPa^{-1}
K_{ea}	effective axial dispersion coefficient, m/s
K_{er}	effective radial dispersion coefficient, m/s
L	length of the bed, m
$\dot{m}_{mix}^j$	mass flow rate of the mixture at heat exchange j, kg/h
N_i	molar flux of component i in r direction, kmol/m^2. s
N_{bed}	number of beds
P	total pressure, kPa
P_i	partial pressure of component i, kPa
Q_j	heat load of heat exchanger j, kW
r	radial coordinate of spherical catalyst pellet, m
r_1	radial dimension in catalyst bed, m
r_2	radial dimension in ceramic support, m
R	university gas constant, kJ/kgmol.K
R_1	inner tube radius, m
R_2	outer radius of composite tube, m
R_p	radius of spherical pellet, m
R_{NH3}	reaction rate of ammonia decomposition, kmol/h m^3
T	temperature, K
T_j	inlet temperature of heat exchanger j, °C
T_f	feed temperature, °C
u_l	axial velocity, m/s
V	reactor volume, m^3
X_i	mole fraction of component i inside catalyst pellet
Y_i	mole fraction of component i
Z	ammonia conversion

Greek letters

α	kinetic parameter
γ_i	generalized stoichiometric coefficient of component i
δ	thickness of hydrogen membrane, μm
ε	porosity of catalyst pellet
ε_1	porosity of catalyst bed
ε_2	porosity of ceramic support
ρ_{mix}	gas density, kg/m^3
η	effectiveness factor
λ	intraparticle porosity
ϕ_i	fugacity coefficient of component i
ω	dimensionless radial coordinate of spherical catalyst pellet

Subscripts

f	feed

Superscripts

B	bulk
c	ceramic support
p	pellet
s	shell side
t	tube side

fuel cells (Uribe et al., 2002; Chellappa et al., 2002; Vilekar et al., 2012). Conventional steam reformers produce inevitably hydrogen with carbon monoxide beyond allowable limits. Therefore, the purity of hydrogen imposes severe constraints on the conventional hydrogen production processes.

In recent years, it has been shown that the implementation of hydrogen perm-selective composite membranes in the new reformer generations have a greater role in solving the problem of hydrogen purity as well as hydrogen yield by selective hydrogen separation and displacement of thermodynamic equilibrium (Collins et al., 1993; Collins and Way, 1993; Hughes, 2001; Dittmeyer et al., 2001; Abashar, 2002; Abashar et al., 2002; Abashar, 2015; Buxbaum and Lei, 2003; Liang and Hughes, 2005; Garcia et al., 2008). However, high pressure driving forces are needed for hydrogen permeation. Further improvements in production, efficient design and operation of these reformers are still needed.

The challenges facing utilization of ultra-clean hydrogen fuel are transportation, delivery, distribution and storage (Alagharu et al., 2010; Di Carlo et al., 2011, 2014; Chiuta et al., 2013). Hydrogen in the gas form requires high pressure vessels (70 MPa) and in a cryogenic liquid form (−253 °C) requires expensive insulated tanks (Zuttel, 2004; Di Carlo et al., 2011). Recently, the on-site (local) hydrogen production and supply has received much attention (Chellappa et al., 2002; Zuttel, 2004; Waghode et al., 2005; Chein et al., 2010; Chiuta et al., 2013; Rizzuto et al., 2014). Liquid methanol (12.50 mass% H_2) and ammonia (17.65 mass% H_2) are competent candidates for the on-site hydrogen production due to their attractive characteristics (high energy density, fewer storage problems, ...etc.) (Metkemeijer and Achard, 1994; Di Carlo et al., 2011). However, reforming of methanol suffers from the problem of carbon oxides (Di Carlo et al., 2014). On the other hand, ammonia is a carbon free compound and in a single step the thermal cracking only gives hydrogen and nitrogen. Moreover, ammonia decomposition process is an economical hydrogen process more than the methanol process (Garcia et al., 2008; Di Carlo et al., 2014). Another attractive

Please cite this article in press as: Abashar, M.E.E. Ultra-clean hydrogen production by ammonia decomposition. Journal of King Saud University – Engineering Sciences (2016), http://dx.doi.org/10.1016/j.jksues.2016.01.002

property of ammonia is lower production cost (1 $/kg) compared with hydrogen (3.5–5.5 $/kg) (Di Carlo et al., 2011). These characteristics grant privilege to ammonia.

Previous theoretical studies on the ammonia decomposition are focused on the removal of toxic ammonia traces as a pollutant (Gobina et al., 1995; Abashar, 2002; Abashar et al., 2002). Remarkable efforts have been done to improve the performance of the catalysts used in ammonia synthesis and decomposition such as iron, nickel, ruthenium (Yin et al., 2004; Cooper and Botte, 2006; Hellman et al., 2009). However, theoretical studies on using ammonia as a feedstock for hydrogen production are limited (Chein et al., 2010) and the modeling and numerical simulation are conducted at the level of experimental bench scale reactors (Sorensen et al., 2006; Chein et al., 2010; Di Carlo et al., 2011, 2014; Rizzuto et al., 2014). More studies are needed for the pilot plants and full scale reactors.

Theoretical studies of multi-stage membrane reactors for the decomposition of ammonia are surprisingly scarce. This study is conducted to gain insight and understanding of ammonia decomposition to produce ultra-clean hydrogen at different levels of a single membrane reactor and multi-stage membrane reactors with inter-stage heating and fresh sweep gas. And, also to evaluate the performance of different reactor configurations. Furthermore, the effects of the key parameters on the performance of the MSFBMR configuration are considered.

2. Reaction kinetics

The decomposition of ammonia is a single step endothermic reaction as follows:

$$NH_3 \rightleftharpoons \frac{1}{2}N_2 + \frac{3}{2}H_2 [\Delta H^o_{298} = 54.6\ \text{kJ/mol}] \tag{1}$$

The reaction rate of ammonia decomposition is given by the following Temkin form (Temkin and Pyzhev, 1940; Dyson and Simon, 1968; Singh and Saraf, 1979; Elnashaie et al., 1988):

$$R_{NH_3} = 5.131 \times 10^{14} \exp\left(-\frac{19656.27}{T}\right) \times \left[\left(\frac{f^2_{NH_3}}{f^3_{H_2}}\right)^{\alpha} - K^2 f_{N_2}\left(\frac{f^3_{H_2}}{f^2_{NH_3}}\right)^{1-\alpha}\right] \tag{2}$$

where f_i is the fugacity of component i and is given by:

$$f_i = \phi_i Y_i P \tag{3}$$

where ϕ_i is the fugacity coefficient of component i, Y_i is the mole fraction of component i and P is the total pressure. The equilibrium constant is given as follows:

$$\log K = 2.6899 + 2001.6 \times T^{-1} + 1.848863 \times 10^{-7} T^2 - 2.691122\ \log T - 5.519265 \times 10^{-5} T \tag{4}$$

where T is the absolute temperature (K).

3. Model development

A two-dimensional model is developed for the decomposition of ammonia. Schematic diagrams of a single fixed bed membrane reactor (FBMR), a cascade of multi-stage fixed bed membrane reactors (MSFBMR) with inter-stage heating and a differential element in the membrane reactor are given in Fig. 1a, b and c, respectively. The following simplifying assumptions are used in the derivation of the conservation equations of the model:

1. The reactor operates at adiabatic steady state conditions.
2. The catalyst particles are isothermal and the external mass and heat transfer resistances are negligible.
3. The membrane has exclusive selectivity for hydrogen.
4. The reactions are considered to take place only in the tube side.
5. Axial dispersion is negligible.
6. A spherical catalyst pellet with symmetric profiles.

3.1. Tube side

The differential mass balance equations on component i gives:

$$\frac{\partial C^t_i}{\partial V} = \frac{D^t_{e_i}\varepsilon_1}{A_o u_l}\frac{1}{r_1}\frac{\partial}{\partial r_1}\left[r_1 \frac{\partial C^t_i}{\partial r_1}\right] + \frac{(1-\varepsilon_1)\gamma_i \eta R_{NH3}}{A_o u_l} \quad 0 < r_1 < R_1, \quad i = 1-3 \tag{5}$$

where i = 1,2 and 3 for NH_3, N_2, and H_2, respectively. γ_i is the generalized stoichiometric coefficient of component i (negative for reactants) .

The boundary conditions are:

$$\begin{aligned} &V = 0 \quad C^t_i = C^t_{if} \\ &r_1 = 0 \quad \frac{\partial C^t_i}{\partial r_1} = 0, \quad i = 1-3 \\ &r_1 = R_1 \quad C^t_i = C^c_i \end{aligned} \tag{6}$$

The effective diffusivity coefficient is calculated from:

$$D_{e_i} = \frac{(1-Y_i)}{\sum_{j\neq i}^{j=1}(Y_i/D_{ij})} \tag{7}$$

3.2. Ceramic support

The differential mass balance equations on component i is given by:

$$\frac{D^c_{e_i}\varepsilon_2}{r_2}\frac{\partial}{\partial r_2}\left[r_2 \frac{\partial C^c_i}{\partial r_2}\right] = 0, \quad R_1 < r_2 < R_2, \quad i = 1-3 \tag{8}$$

The boundary conditions are:

$$\begin{aligned} &r_2 = R_1, \quad C^t_i = C^c_i, \quad D^t_{e_i}\varepsilon_1 \left.\frac{\partial C^t_i}{\partial r_1}\right|_{r_1=R_1} = D^c_{e_i}\varepsilon_2 \left.\frac{\partial C^c_i}{\partial r_2}\right|_{r_2=R_1}, \quad i = 1-3 \\ &r_2 = R_2, \quad \left.\frac{\partial C^c_i}{\partial r_2}\right|_{r_2=R_2} = 0, \quad i = 1,2 \end{aligned} \tag{9}$$

for H_2:

$$\left.\frac{\partial C^c_3}{\partial r_2}\right|_{r_2=R_2} = \left(\frac{28.84 \times 10^{-5} \exp\left(-\frac{1888.381}{T}\right)}{\delta D^c_{e_3}\varepsilon_2}\right)\left[\sqrt{P^t_{H_2}} - \sqrt{P^s_{H_2}}\right] \tag{10}$$

and energy balance equation is given by:

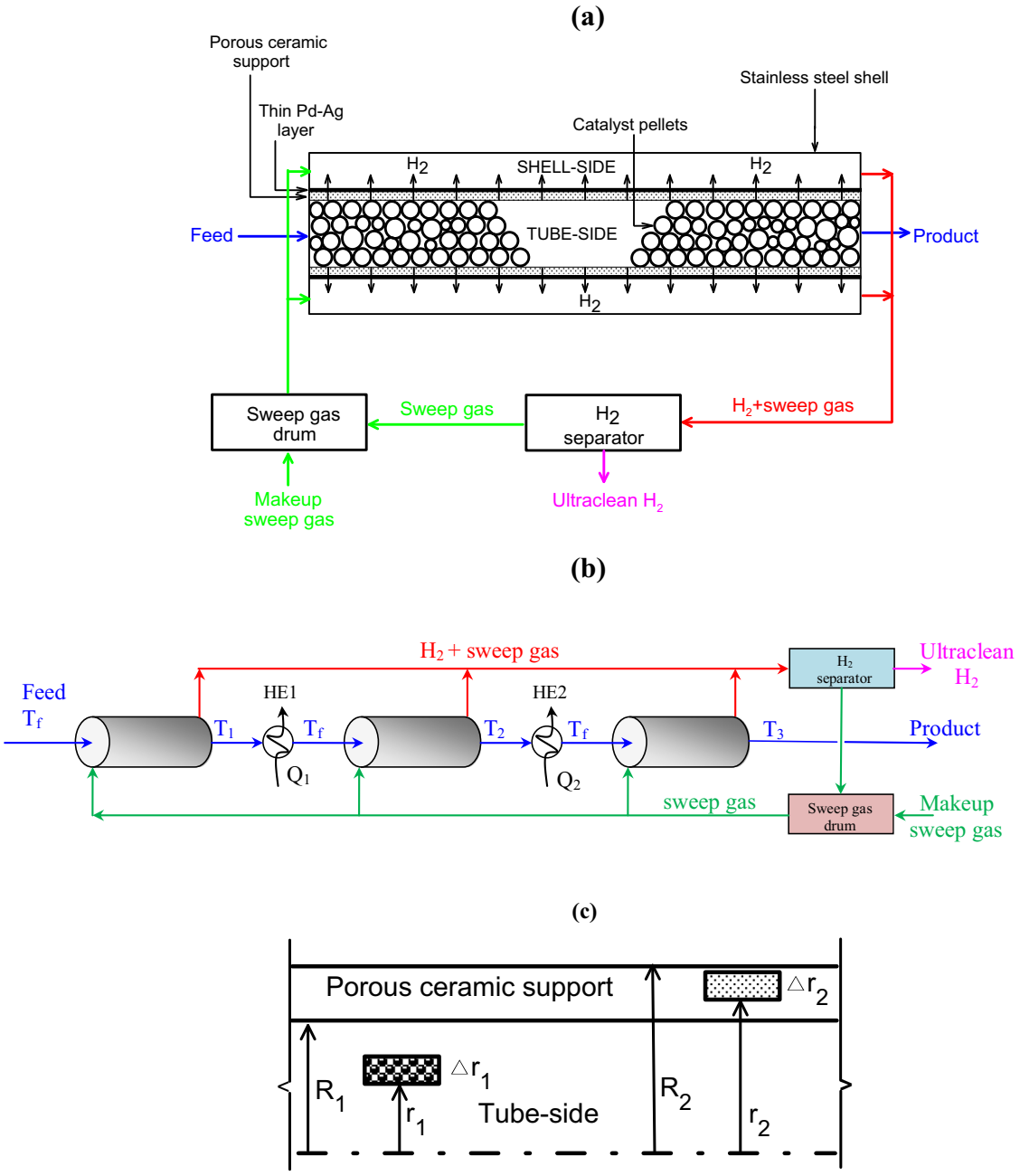

Figure 1 Schematic representation: (a) single fixed bed membrane reactor (FBMR); (b) multi-stage fixed bed membrane reactors (MSFBMR); (c) differential element in the membrane reactor.

$$\varepsilon_1 u_l \rho_{mix} C_{pmix} A_o \frac{\partial T}{\partial V} = \varepsilon_1 K_{ea} \frac{\partial^2 T}{\partial l^2} + \varepsilon_1 K_{er} \frac{1}{r_1} \frac{\partial}{\partial r_1} \left[r_1 \frac{\partial T}{\partial r_1} \right] + (-\Delta H)\eta(1-\varepsilon_1) R_{NH_3} \quad (11)$$

The boundary conditions are:

$$\begin{aligned} &V = 0 \quad T = T_f \\ &V = V_o \quad \frac{\partial T}{\partial V} = 0 \\ &r_1 = 0 \quad \frac{\partial T}{\partial r_1} = 0 \\ &r_1 = R_1 \quad \frac{\partial T}{\partial r_1} = 0 \end{aligned} \quad (12)$$

The conversion of ammonia is given by:

$$Z = 1 - \frac{F_{NH_3}}{F^o_{NH_3}} \quad (13)$$

3.3. Catalyst pellet and effectiveness factor

A differential molar balance inside a porous catalyst pellet on component i gives:

$$\frac{1}{r^2} \frac{d}{dr}(r^2 N_i) = \gamma_i \frac{R_{NH3}(X_i, T, P)}{(1-\varepsilon)} \quad (14)$$

subject to boundary conditions :

$$r = 0 \quad N_i = 0$$
$$r = R_p \quad X_i = X_i^b \tag{15}$$

Using lengthy manipulation, the following intraparticle dimensionless molar balance equation for the catalyst pellet is obtained:

$$\frac{d^2X_i}{d\omega^2} + \frac{2}{\omega}\frac{dX_i}{d\omega} - \frac{1}{(X_i - \gamma_i)}\left(\frac{dX_i}{d\omega}\right)^2 = -\gamma_i \frac{R_p^2}{CD_{ie}}\left(1 - \frac{X_i}{\gamma_i}\right)\frac{R_{NH3}(X_i, T, P)}{(1-\varepsilon)} \tag{16}$$

with boundary conditions as:

$$\omega = 0 \quad \frac{dX_i}{d\omega} = 0$$
$$\omega = 1.0 \quad X_i = X_i^b \tag{17}$$

where ω ($\omega = r/R_p$) is the dimensionless coordinate, C is the total concentration and D_{ie} is the effective diffusion coefficient of component i. The effective diffusion coefficient is given by (Elnashaie et al., 1988):

$$D_{ei} = \frac{1}{2}\varepsilon D_i \tag{18}$$

where ε is the intraparticle porosity and D_i is bulk diffusion coefficient of component i. The bulk diffusion coefficient is given by:

$$D_i = D_i^o\left(\frac{T}{273}\right)^{1.75}\frac{1}{P} \tag{19}$$

The diffusion coefficient of component i (D_i^o) at 0 °C and 1 atm is given by:

$$D_i^o = \frac{1 - X_i^b}{\sum_{j=1}^{n}(X_i^b/D_{ji}^o) - (X_i^b/D_{ii}^o)} \tag{20}$$

and X_i is given by:

$$X_i = \gamma_i - (\gamma_i - X_i^b)\left[\frac{\gamma_j - X_j}{\gamma_j - X_j^b}\right]^{D_{je}/D_{ie}} \tag{21}$$

The effectiveness factor is used as a measure of diffusion resistances inside the catalyst pellet and defined as the actual overall rate of reaction divided by the rate of reaction at the bulk (surface) conditions.

$$\eta = \frac{\int_0^{R_p} r^2 R_{NH3}(\mathbf{X}, T, P)dr}{\int_0^{R_p} r^2 R_{NH3}^b(\mathbf{X}^b, T^b, P^b)dr} \tag{22}$$

where $\mathbf{X}$ is the vector of mole fractions, $\mathbf{X}^b$ is the vector of mole fractions at the bulk conditions and R_p is the radius of the catalyst pellet.

3.4. Membrane side

The differential material balance for hydrogen in the permeation side gives (Shu et al., 1994):

$$\frac{dF_{H_2}^p}{dV} = \left(\frac{28.84 \times 10^{-5}}{\delta d_{H_2}}\right)\exp\left(-\frac{1888.381}{T}\right)\left(\sqrt{P_{H_2}^r} - \sqrt{P_{H_2}^p}\right) \tag{23}$$

3.5. Inter-stage heat load

The inter-stage heat load per j heat exchanger is calculated by the following equation:

$$Q_j = \dot{m}_{mix}^j C_{Pmix}^j (T_f - T_j) \tag{24}$$

The cumulative heat load is the sum of the inter-stage heat loads ($\sum Q_j$).

4. Solution algorithm

Data for simulation are presented in Table 1. The global orthogonal collocation technique (Villadsen and Michelsen, 1978) is implemented to change the set of the partial differential into a set of ordinary equations. Then, the new set of ordinary differentials is integrated by an IMSL subroutine (DGEAR) based on a Runge–Kutta–Verner fifth and sixth-order method with automatic step size and double precision to ensure accuracy. The two-point boundary value differential equations of the catalyst pellet are discretized by the global orthogonal technique to give a set of nonlinear algebraic equations. These nonlinear algebraic equations are solved numerically by an IMSL subroutine called ZSPOW. A special technique has been applied for the initial guesses to ensure the convergence of the equations to the desired level of accuracy. The technique started from one collocation point and the solution of the one collocation point is utilized to find the initial guesses for the two collocation points and so on. Three collocation points are adopted in this study, since more than three collocation points give almost the same profiles inside the catalyst pellet.

5. Results and discussion

According to Le Châtelier's principle the position of a chemical equilibrium is controlled by the changes of concentration, pressure and temperature. In the case of ammonia decomposition, the reaction is endothermic and reversible with increasing number of moles. Hence, the ammonia equilibrium conversion increases with increase of temperature, decrease of pressure and removal of products. Moreover, the increase of temperature also has a positive effect on the kinetics by increasing the rate of ammonia decomposition. Hence, for a reactor without membrane it is desirable to work at low pressures and high

Table 1 Data used for simulation.

Feed composition	Mol%
NH_3	95.00
H_2	3.00
N_2	2.00
Reactor	
Volume of the catalyst bed (m^3)	0.1
Diameter of bed (m)	0.2
Membrane thickness (μm)	3.0
Diameter of catalyst pellet (m) 3.0×10^{-3}	
Void fraction	0.46
Pressure of sweep gas stream (bar)	1.0

temperatures. However, excessive temperatures have destructive effects on the catalyst and the reactor. In the case of the membrane reactor the increase of pressure has two opposing effects of shifting the equilibrium to the right by enhancing the permeation of hydrogen and to the left by decreasing the number of moles to form ammonia. Therefore, the direction of the equilibrium is controlled by the dominant force.

In this study the single reactor configuration is considered first. Fig. 2a shows exit ammonia conversion as a function of pressure obtained by a single fixed bed membrane reactor (FBMR).The profile shows a minimum value at $P = 8.342$ due to the two competing forces. It is clearly shown that, the exit ammonia conversion decreases with the increase of the pressure due to its negative influence on the thermodynamic equilibrium to a critical inflection point beyond which the role of the membrane comes to dominate and developing an effective permeation zone. As it can be seen that the operating pressure must be in the effective permeation zone i.e. $P > 8.342$ bar. The operating pressure selected for this study is 40.0 bar around the value given by Rahimpour and Asgari (2009). Note that this critical point needs to be identified at various operating conditions to determine the critical minimum operating pressure.

In order to select an appropriate reactor volume throughout this study, the rate of ammonia reaction in the fixed bed membrane reactor (FBMR) at 40.0 bar is presented in Fig. 2b. As it can be seen in Fig. 2b, that the reaction is very fast and the rate of ammonia reaction drops drastically to a low value. This figure shows that the part of reactor beyond 0.1 m^3 seems to have an insignificant effect. Therefore, a reactor volume of 0.1 m^3 is adopted in the rest of this study.

Fig. 3a compares the performance of a single fixed bed reactor (FBR) and a fixed bed membrane reactor (FBMR). It is clearly shown that the exit ammonia conversion is significantly enhanced by the FBMR i.e. the exit ammonia conversion is increased by 60.48% from 13.03% obtained by the FBR to 20.91% obtained by the FBMR. Despite the fact that the membrane plays the main role in the displacement of the thermodynamic equilibrium and achieving a high ammonia conversion, at the same time causing a severe drop in temperature along the length of the reactor as shown in Fig. 3b. The drop in the temperature has a negative effect on the kinetics and limited further improvement in the exit ammonia conversion.

Fig. 3c shows hydrogen concentration profiles along the length of the FBR and FBMR. A build up of hydrogen concentration along the FBR is shown, while a drastic drop in hydrogen concentration occurs along the length of the FBMR due to hydrogen permeation. It seems that the hydrogen permselective membrane is very effective in removing hydrogen from the reaction media and displacement of the thermodynamic equilibrium. The comparison also shows that the reactor product from the FBMR is an ultra-clean hydrogen and also high grade nitrogen products which can be used as a feedstock for other industries.

The effectiveness factor profiles along the length of the FBR and FBMR are depicted in Fig. 3d. The value of the effectiveness factor is used to indicate the magnitudes of reaction and diffusion limitations. As it can be seen in Fig. 3d that at the beginning of the reactor the effectiveness factor is low indicating that the intraparticle diffusion has a strong effect on the rate of reaction i.e. the reaction is diffusion limited. This is practically implied that the outer surface of catalyst pellet is effective. This could be due to the fast reaction at the pellet surface relative to the diffusion caused by the high feed temperature at the entrance of each bed. Then, the effectiveness factor jumps drastically to flat profiles that have a value of almost unity indicating that the reaction is limited by the kinetics at the surface of the catalyst pellet due to the low temperature at the surface. This result indicates that under the operating conditions in this study, the homogeneous model can be implemented as a good approximation without solving the catalyst pellet nonlinear two-point boundary value equations along the length of the reactor. The effectiveness factor profile for the FBMR is higher than the FBR due the fact that the surface reaction of the FBMR is less than the FBR due to the lower temperature profile as shown in Fig. 3b.

The effect of the feed temperature along the length of the FBMR is shown in Fig. 4a. A feed temperature range (600 °C–900 °C) is considered (Chiuta et al., 2013; Di Carlo et al., 2014). As shown in Fig. 4a, a substantial increase in ammonia conversion is achieved by increasing the feed

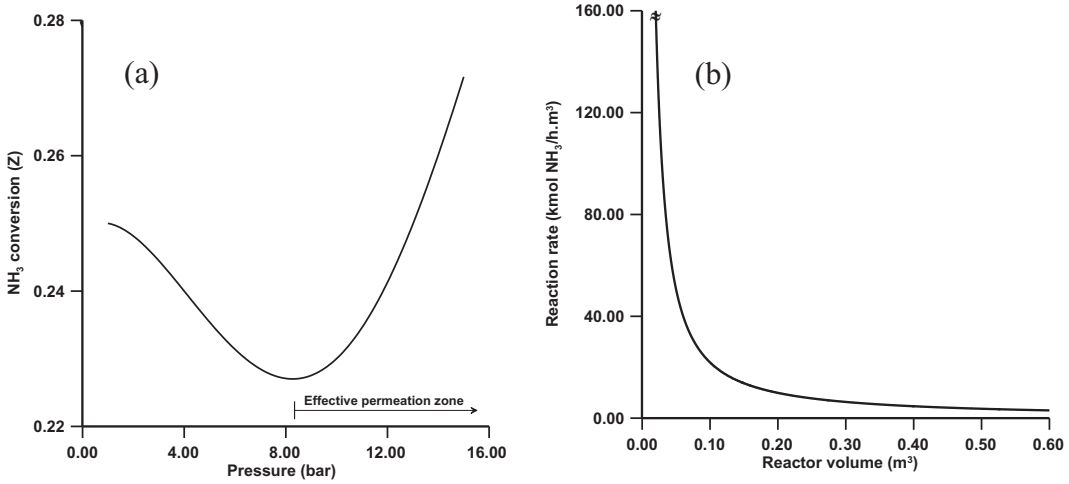

Figure 2 (a) NH_3 conversion as a function of pressure; (b) Reaction rate along the length of the reactor.

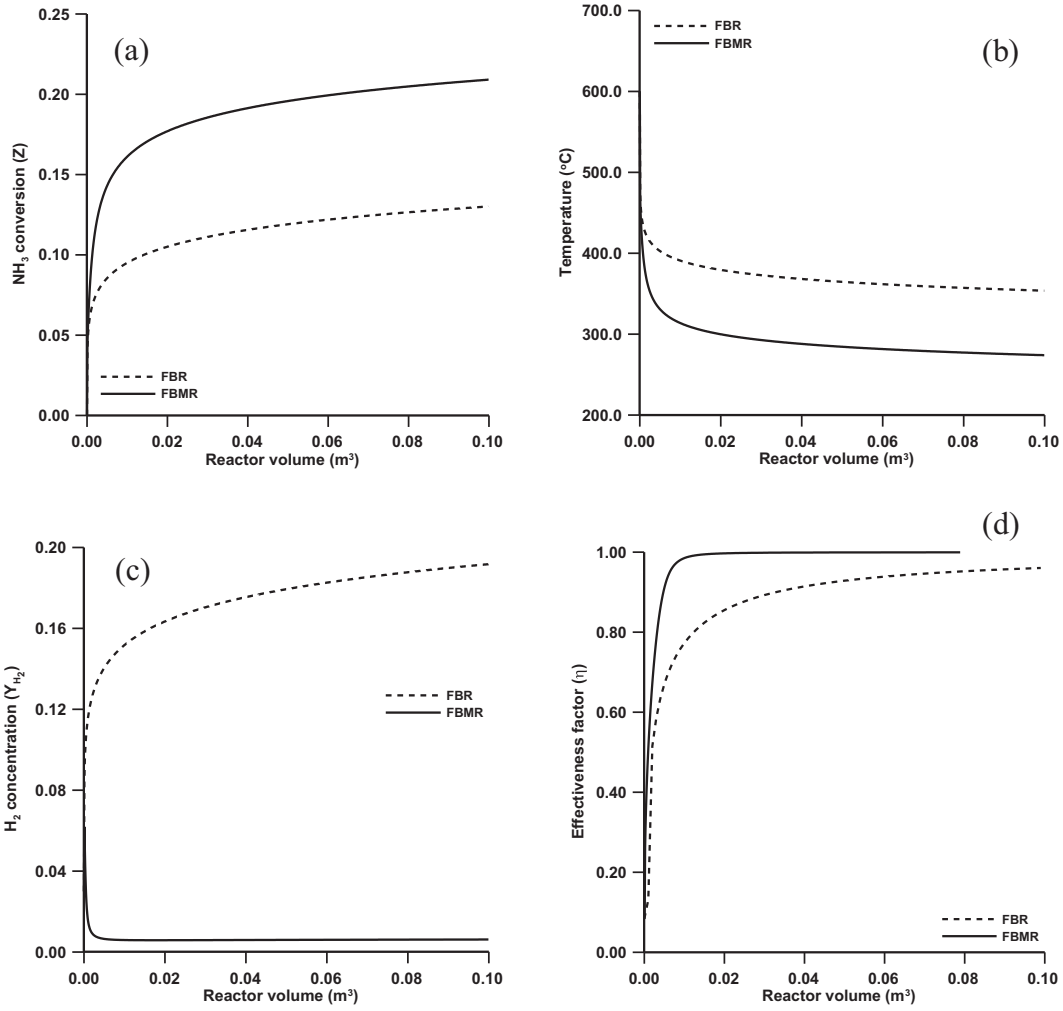

Figure 3 Comparison of different reactor configurations. (a) NH_3 conversion profiles along the length of the FBR and FBMR; (b) temperature profiles along the length of the FBR and FBMR; (c) hydrogen concentration profiles along the length of the FBR and FBMR; (d) effectiveness profiles along the length of the FBR and FBMR.

temperature. About 91.20% increase in ammonia conversion is obtained from 20.91% to 36.98%, when the feed temperature is increased from 600 °C to 900 °C. It is interesting to note that the effect of feed temperature on the ammonia conversion at high values is more pronounced than at low values. For example the increase of ammonia conversion is about 11.57% when the feed temperature is increased from 600 °C to 700 °C and about 32.63% when the feed temperature is increased from 800 °C to 900 °C. Fig. 4b shows the ammonia conversion as a function of temperature at different feed temperatures. As one can see that the exit low temperature in the vicinity of the equilibrium is obtained by all cases. In this situation, the performance of the FBMR is controlled by the kinetics and virtually weak hydrogen permeation. The corresponding mole fractions of the components NH_3, H_2 and N_2 are shown in Fig. 4c. The ammonia and hydrogen concentrations show inflection points of minimum and maximum value, respectively. This behavior is caused by the effect of ammonia consumption and hydrogen permeation on the total number of moles that prevail along the length of the reactor.

From the above discussion the single reactor configuration of the FBMR failed to achieve complete decomposition of ammonia due to the exit low temperature. Since the kinetics limits the performance of the FBMR at a low temperature, the idea of a multi-stage configuration (MSFBMR) with inter-stage heating is considered. In this configuration each bed has a volume of 0.1 m^3. The MSFBMR configuration achieves 100% ammonia conversion by three beds and a small final bed (Bed_4) of a volume of 0.011 m^3 as shown in Fig. 5a . It is obvious that this configuration works remarkably well beyond the thermodynamic equilibrium due to the imposed membrane as shown in beds 2 and 3.

Fig. 5b shows the hydrogen molar flow rate in the reaction and permeation sides for the MSFBMR configuration. As it can be shown that the hydrogen permeation is high in the first bed and decreases progressively to the last bed, this could be due to the availability of the hydrogen in the reaction side.

Fig. 6a shows the effect of the feed temperature on the number of beds that required to achieve 100% ammonia conversion. As it can be seen, that significant reduction in beds is

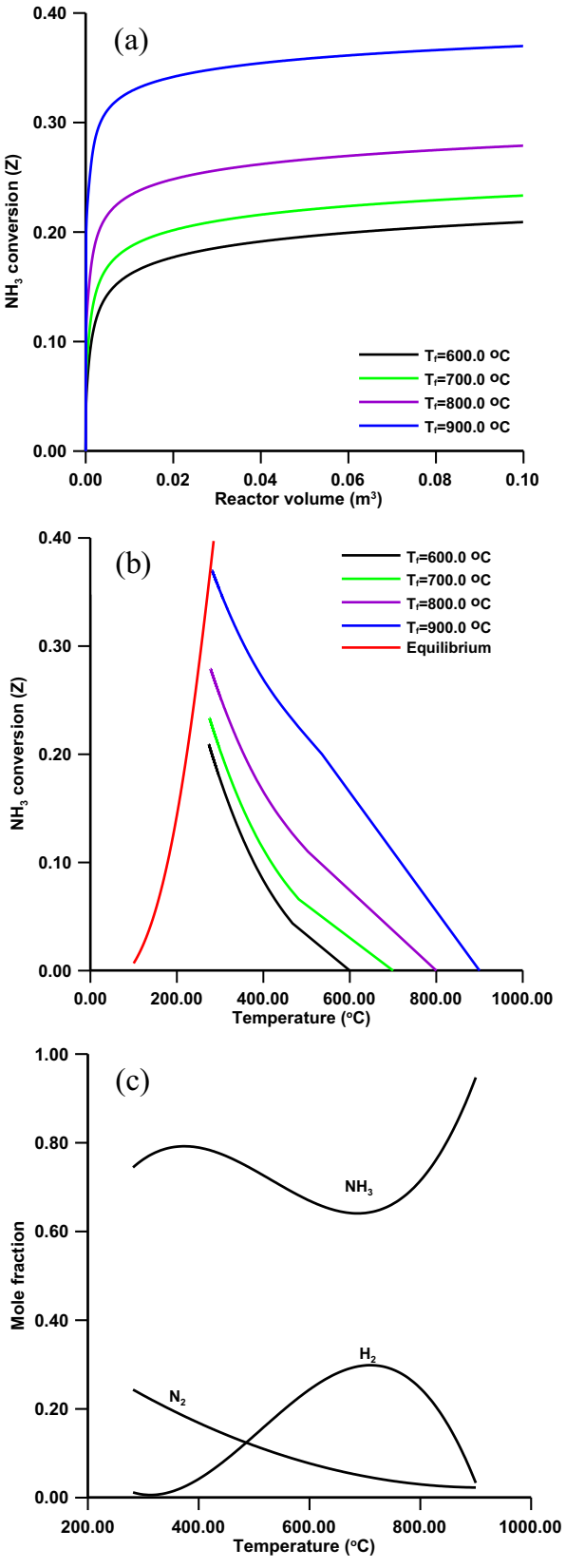

Figure 4 FBMR configuration. (a) profiles of NH_3 conversion along the length of the reactor for various feed temperatures; (b) NH_3 conversion as a function of temperature for various feed temperatures; (c) concentration of NH_3, H_2 and N_2 as a function of temperature.

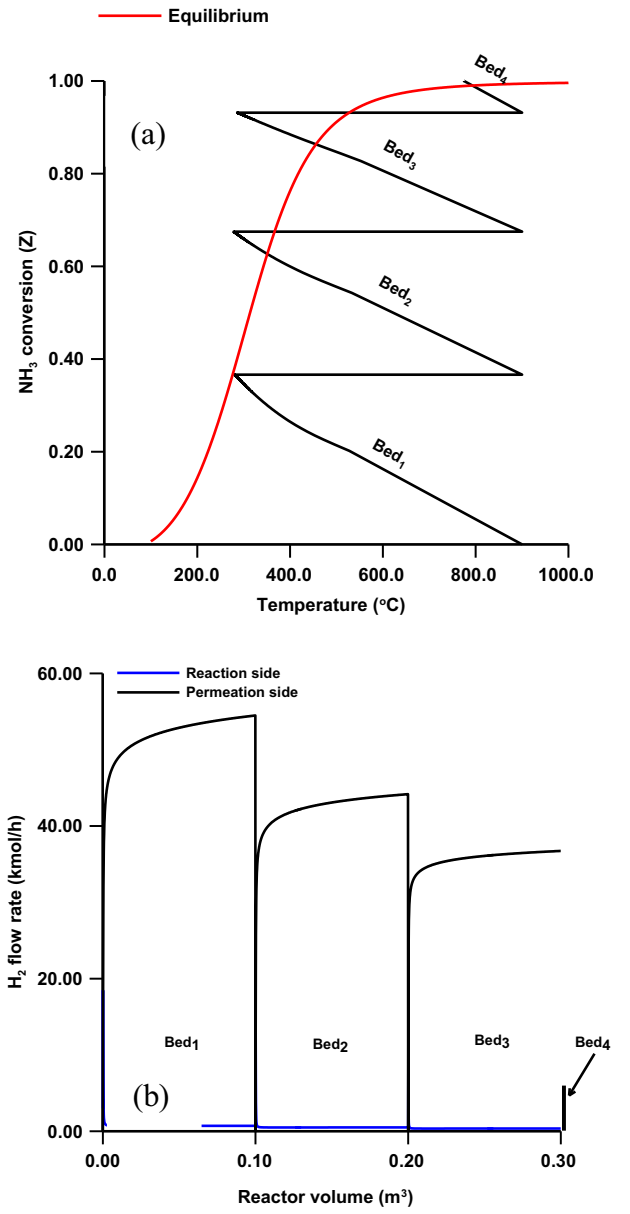

Figure 5 MSFBMR configuration. (a) complete ammonia conversion by interstage heating; (b) profiles of hydrogen flow rate in the reaction and permeation sides.

achieved by increasing the feed temperature. The number of the beds seems to decrease linearly with the feed temperature as shown in Fig. 6b. An empirical equation of the form is obtained:

$$N_{bed} = -0.01 T_f\ (^{\circ}\mathrm{C}) + 13 \tag{25}$$

This equation can predict satisfactorily the number of beds.

In Fig. 6c the profile of heat load per interstage heat exchanger is plotted for the case of four bed configuration. In this case three interstage heat exchangers are required. The profile shows an inflection point of a maximum nature. The heat load is a function of the mass flow rate and heat capacity of the gas mixture as well as the drop of the temperature along the heat exchanger. All these quantities vary from heat exchanger to another causing this maximum point.

Please cite this article in press as: Abashar, M.E.E. Ultra-clean hydrogen production by ammonia decomposition. Journal of King Saud University – Engineering Sciences (2016), http://dx.doi.org/10.1016/j.jksues.2016.01.002

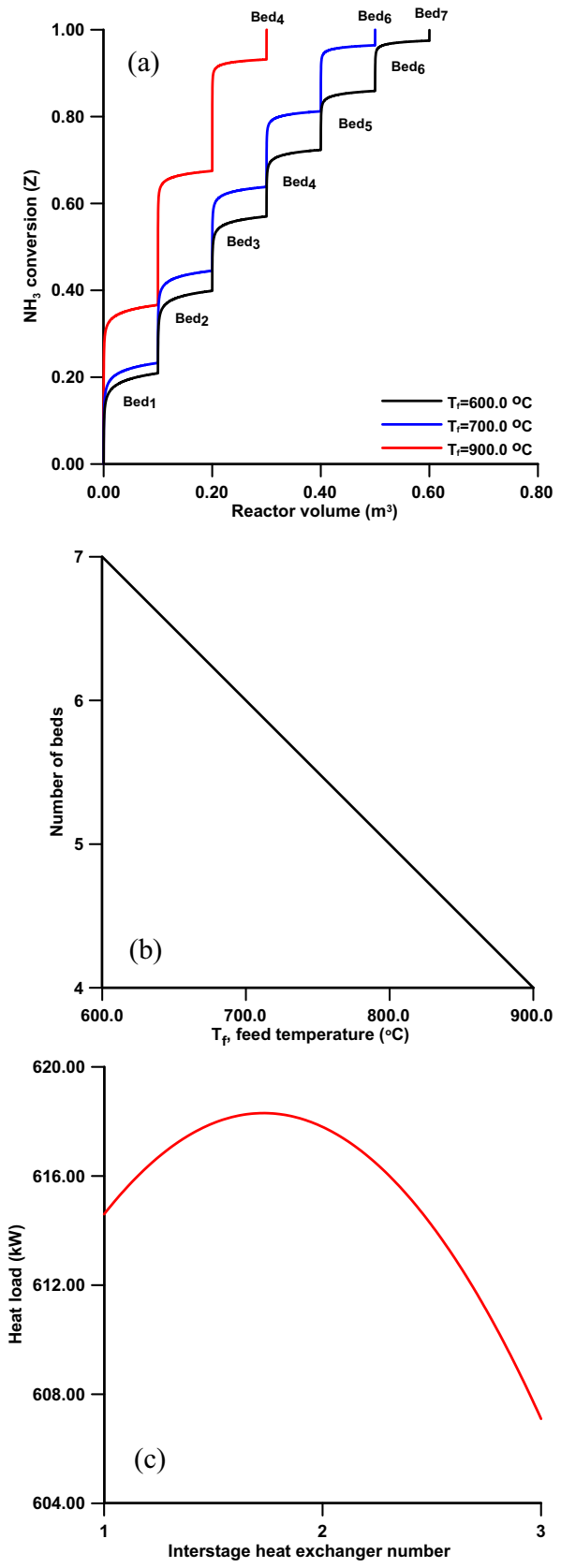

Figure 6 MSFBMR configuration. (a) NH_3 conversion as a function of feed temperature; (b) number of beds as a function of feed temperature; (c) heat load as a function of number of interstage heat exchangers.

6. Conclusions

Ammonia decomposition is an attractive carbon free single step process for the production of hydrogen. In this paper, the conducted numerical simulation has shown that the multi-stage membrane reactors (MSFBMR) for ammonia decomposition have significant advantages over the single fixed bed membrane reactor (FBMR). Also, the MSFBMRs have attractive potential application for the efficient production of ultra-clean hydrogen suitable for the PEM fuel cells. The results suggested that the multi-stage configuration is suitable for the on-site hydrogen production. The hydrogen membrane, number of beds and the inter-stage heat exchangers strongly influenced the performance of the MSFBMR. Since, the diffusion limitations effect is shown to be confined to very small regions in each bed a pseudo-homogeneous model can be utilized as an initial trial model to extract some features of the process. The results of this preliminary study might have fundamental importance in designing of the MSFBMR for the ammonia decomposition. Optimization of this process will be addressed in future research. To this end, the compelling merits of the MSFBMR dedicate that intensive efforts are still needed in academia and industry levels.

Acknowledgements

This project was supported by King Saud University, Deanship of Scientific Research, College of Engineering Research Center.

References

Abashar, M.E.E., 2002. Integrated catalytic membrane reactors for decomposition of ammonia. Chem. Eng. Process. 41, 403–412.
Abashar, M.E.E., Al-Sughair, Y.S., Al-Mutaz, I.S., 2002. Investigation of low temperature decomposition of ammonia using spatially patterned catalytic membrane reactors. Appl. Catal. A 6124, 1–20.
Abashar, M.E.E., 2015. Parametric sensitivity analysis to investigate heptane reforming in circulating fast fluidized bed membrane reactors. J. King Saud Univ. – Eng. Sci. 27, 1–13.
Alagharu, V., Palanki, S., West, K.N., 2010. Analysis of ammonia decomposition reactor to generate hydrogen for fuel cell applications. J. Power Sources 195, 829–833.
Buxbaum, R.E., Lei, H., 2003. Power output and load following in a fuel cell fueled by membrane reactor hydrogen. J. Power Sources 123 (1), 43–47.
Collins, J.P., Way, J.D., Kraisuwansarn, N., 1993. A mathematical model of a catalytic membrane reactor for decomposition of NH3. J. Membr. Sci. 177 (2–3), 265–282.
Collins, J.P., Way, J.D., 1993. Investigation of low temperature decomposition of ammonia using spatially patterned catalytic membrane reactors. J. Membr. Sci. 77, 265–282.
Chellappa, A.S., Fischer, C.M., Thomson, W.J., 2002. Ammonia decomposition kinetics over Ni-Pt/Al_2O_3 for PEM fuel cell applications. Appl. Catal. A-Gen. 227, 231–240.
Cooper, M., Botte, G.G., 2006. Hydrogen production from the electrooxidation of ammonia catalyzed by Platinum and Rhodium on Raney Nickel substrate. J. Electrochem. Soc. 153 (10), A1894–A1901.
Chein, R.Y., Chen, Y.C., Chang, C.S., Chung, J.N., 2010. Numerical modelling of hydrogen production from ammonia decomposition for fuel cell applications. Int. J. Hydrogen Energy 35, 589–597.

Chiuta, S., Everson, R.C., Neomagus, H.-W.J.P., Gryp, P., Bessarabov, D.G., 2013. Reactor technology options for distributed hydrogen generation via ammonia decomposition: a review. Int. J. Hydrogen Energy 38, 14968–14991.

Dyson, D.C., Simon, J.M., 1968. A kinetic expression with diffusion correction for ammonia synthesis on industrial catalyst. Ind. Eng. Chem. Fundam. 7, 605–610.

Dittmeyer, R., Hollein, V., Daub, K., 2001. Membrane reactors for hydrogen and dehydrogenation processes based on supported palladium. J. Mol. Catal. 173, 135–184.

Di Carlo, A., Dell'Era, A., Del Prete, Z., 2011. 3D simulation of hydrogen production by ammonia decomposition in a catalytic membrane reactor. Int. J. Hydrogen Energy 36, 11815–11824.

Di Carlo, A., Dell'Era, A., Del Prete, Z., 2014. Ammonia decomposition over commercial Ru/Al2O3 catalyst: An experimental evaluation at different operative pressures and temperatures. Int. J. Hydrogen Energy 39, 808–814.

Elnashaie, S.S., Abashar, M.E., Al-Ubaid, A.S., 1988. Simulation and optimization of an industrial ammonia reactor. Ind. Eng. Chem. Res. 27, 2015–2022.

Farrell, C.G., Gardner, C.L., Ternan, M., 2007. Experimental and modelling studies of CO poisoning in PEM fuel cells. J. Power Sources 171, 282–293.

Gobina, E.N., Oklany, J.S., Hughes, R., 1995. Elimination of ammonia from coal gasification streams by using a catalytic membrane reactor. Ind. Eng. Chem. Res. 34, 3777–3783.

Garcia, F.R., Hua-Ma, Y., Rodriguez-Ramos, I., Guerrero-Ruiz, A., 2008. High purity hydrogen production by low temperature catalytic ammonia decomposition in a multifunctional membrane reactor. Catal. Commun. 9, 482–486.

Hughes, R., 2001. Composite palladium membranes for catalytic membrane reactors. Membr. Tech. 131, 9–13.

Hellman, A., Honkala, K., Remediakis, I.N., Logadottir, A., Carlsson, A., Dahl, S., 2009. Ammonia synthesis and decomposition on a Ru-based catalyst modeled by first principles. Surf. Sci. 603 (10–12), 1731–1739.

Liang, W., Hughes, R., 2005. The catalytic dehydrogenation of isobutane to isobutene in a palladium/silver composite membrane reactor. Catal. Today 104, 238–243.

Metkemeijer, R., Achard, P., 1994. Comparison of ammonia and methanol applied indirectly in a hydrogen fuel cell. Int. J. Hydrogen Energy 19, 535–542.

Oetjen, H.F., Schmidt, V.M., Stimming, U., Trila, F.J., 1996. Performance data of a proton exchange membrane fuel cell using H_2/CO as fuel gas. J. Electrochem. Soc. 143, 3838–3842.

Rahimpour, M.R., Asgari, A., 2009. Production of hydrogen from purge gases of ammonia plants in a catalytic hydrogen-permselective membrane. Int. J. Hydrogen Energy 39, 5795–5802.

Rizzuto, E., Palange, P., Del Prete, Z., 2014. Characterization of an ammonia decomposition process by means of a multifunctional catalytic membrane reactor. Int. J. Hydrogen Energy 39, 11403–11410.

Singh, C.P.P., Saraf, D.N., 1979. Simulation of ammonia synthesis reactors. Ind. Eng. Chem. Process. Des. Dev. 18, 364–370.

Shu, J., Bernard, P.A.G., Kaliaguine, S., 1994. Methane steam reforming in asymmetric Pd-and Pd-Ag/porous ss membrane reactors. Appl. Catal. A 119, 305–325.

Sorensen, R.Z., Klerke, A., Quaade, U., Jensen, S., Hansen, O., Christenssen, C.H., 2006. Promoted Ru on high surface area graphite for efficient miniaturised production of hydrogen from ammonia. Catal. Lett. 112 (1–2), 77–81.

Temkin, M., Pyzhev, V., 1940. Kinetics of the synthesis of ammonia on promoted iron catalysts. Acta. Physicochim. URRS 12, 327–335.

Uribe, F.A., Gottesfeld, S., Zawodzinski, T.A., 2002. Effect of ammonia as potential fuel impurity on proton exchange membrane fuel cell performance. J. Electrochem. Soc. 149, A293–A296.

Villadsen, J.V., Michelsen, M.L., 1978. Solution of Differential Equations Models by Polynomial Approximation. Prentice-Hall, Inc., Englewood Cliffs, N.J..

Vilekar, S.A., Fishtik, I., Datta, R., 2012. The peculiar catalytic sequence of the ammonia decomposition reaction and its steady-state kinetics. Chem. Eng. Sci. 71, 333–344.

Waghode, A.N., Hanspal, N.S., Shigidi, I.M., Nassehi, V., Hellgardt, K., 2005. Computer modelling and numerical analysis of hydrodynamics and heat transfer in non-porous catalytic reactor for the decomposition of ammonia. Chem. Eng. Sci. 60, 5862–5877.

Yin, S.F., Xu, B.Q., Zhou, X.F., Au, C.T., 2004. A mini-review on ammonia decomposition catalysts for on-site generation of hydrogen for fuel cell applications. Appl. Catal. A 277, 1–9.

Zuttel, A., 2004. Hydrogen storage methods. Naturwissenschaften 91, 157–172.

Zamel, N.L.X., 2013. Effective transport properties for polymer electrolyte membrane fuel cells-With a focus on the gas diffusion layer. Prog. Energy Combust. Sci. 39, 111–146.

Please cite this article in press as: Abashar, M.E.E. Ultra-clean hydrogen production by ammonia decomposition. Journal of King Saud University – Engineering Sciences (2016), http://dx.doi.org/10.1016/j.jksues.2016.01.002